Fast Exfoliation and Functionalisation of 2D Crystalline Carbon Nitride by Framework Charging

Jingjing Jia, Edward R. White, Adam J. Clancy, Noelia Rubio, Theo Suter, Thomas S. Miller, Paul F. McMillan, Veronika Brázdová, Furio Corà, Chris A. Howard, Robert V. Law, Cecilia Mattevi,* and Milo S. P. Shaffer*

Abstract: 2D layered graphitic carbon nitride nanosheets offer tunable electronic and chemical properties. However, exfoliation and functionalisation of gCN for specific applications remains challenging. We report a scalable one-pot reductive method to produce solutions of single and few layer 2D gCN nanosheets with excellent stability in a high mass yield (35%) from polytriazine imide. High resolution imaging confirms the intact crystalline structure and identifies an AB stacking. The first successful deliberate organic functionalisation of dissolved gCN is illustrated, providing a general route to adjust their properties.

Graphitic carbon nitride (gCN) has triggered tremendous interest due to its 2D structure, analogous to graphene, but with complementary characteristics.[1] In particular, it offers inherent semiconductivity with tunable band gap and optical absorption,[2] whilst the different chemical valences of N and C create empty sites within the layers.[3] Monolayer/few layer carbon nitride nanosheets (FL-CNs) have been isolated as a new family of 2D layered materials, motivated by their unique photocatalytic activity.[4] Several methods have been adopted to synthesize FL-CNs of various thicknesses/sizes.[5] Unfortunately, many of these processes damage the structure, altering the properties of interest; they are also time-consuming and provide low yields and dilute suspensions, and most work has focused on the disordered heptazine-based gCNs. Polytriazine imide (PTI) has been previously synthesized and characterized using a number of bottom-up approaches.[6] PTI is more crystalline than its heptazine-based counterpart, containing genuine planar layers of imide-bridged triazine units,[7] and its exfoliation into high quality 2D FL-CN crystals is, therefore, attractive. Achieving a non-damaging preparation of 2D few-layered PTI (FL-PTI) in a high yield is still in its infancy, although slow dissolution has recently been reported.[8] Moreover, while covalent functionalisation is a vital tool in tailoring the properties of nanomaterials,[9] to date there has been little direct covalent functionalisation of PTI.

This paper demonstrates a simple, one-pot exfoliation, dissolution, and optional functionalisation of FL-PTI *via* reduction. Reductive charging has been used previously to dissolve a variety of 2D nanomaterials,[10] *via* metal-ammonia solutions and organic charge transfer agents (CTA). The use of sodium naphthalide (NaNp) dissolved in N,N-dimethylacetamide (DMAc) was recently found to be especially effective for the dissolution and functionalisation of single wall nanotubes in a single step.[14] Here the methodology is adapted to gCNs, specifically PTIs. Successful exfoliation of PTI was achieved by framework charging process (Fig. 1). Sodium is used as the electron source to form naphthalide ions, which act as a CTA. DMAc is an excellent room temperature solvent for naphthalene/ide and anionic nanocarbons, and can be expected to be a good solvent for FL-PTI.[11] NaNp/DMAc solution has a characteristic green color which simplifies reaction monitoring. NaNp/DMAc solutions were added into dried PTI powders at controlled stoichiometry. The reduction and exfoliation process was observed by the color change from the initial brown PTI suspension to dark green after addition of NaNp/DMAc, before finally forming a brilliant orange dispersion of FL-PTI (FL-PTI^{n-}) within minutes (Fig. S1). After removing the remaining insoluble PTI fragments by centrifugation (5000 g, 30 min, Fig. S2), a homogeneous golden FL-PTI^{n-} solution with a concentration up to 1.2 mg·mL^{-1} was obtained (Fig. S1c), which was stable under N_2 for >1 year (Fig. S3a). Deposited FL-PTI^{n-} nanosheets display hexagonal geometry with a height of 1-2 nm (Fig. S3), indicating that they comprise only a few PTI layers, based on a 3.52 Å layer thickness.[6b] The negative charges from the naphthalide are likely to be rapidly transferred to the PTI, due to the high reduction potential of naphthalide (*ca.* 3.0 eV vs SHE);[12] accelerated by the small size of the PTI platelets and the intrinsic pores.[13] The partially dissociated Na$^+$ counterions leave a net unscreened negative charge on the PTI^{n-} (Fig. S4a), leading to short range Coulombic repulsions and hence exfoliation of PTI into solvated FL-PTI^{n-} sheets (Fig. 1), analogous to reduced nanocarbons[10a, 14] and transition metal dichalcogenides.[10b] Upon air exposure, the FL-PTI reagglomerate slowly (~2 months, Fig. S5b); the reduced rate compared to charged SWCNTs,[14b] likely relates to the lower aspect ratio and localisation/low mobility of the charges on the framework.[15]

[*]   J. Jia, E. R. White, A. J. Clancy, N. Rubio, M. S. P. Shaffer,
       Dept. Chemistry, Imperial College London,
       London, SW7 2AZ, UK.
       E-mail: m.shaffer@imperial.ac.uk
       C. Mattevi
       Dept. Materials, Imperial College London,
       London, SW7 2AZ, UK
       E-mail: c.mattevi@imperial.ac.uk
       T. Suter, T. S. Miller, P. F. McMillan,
       V. Brázdová, F. Corà,
       Dept. Chemistry, University College London,
       London, WC1H 0AJ, UK.
       C. A. Howard
       Dept. Physics and Astronomy, University College London,
       London, WC1E 6BT, UK.

80

81 **Figure 1.** Schematic of charging and exfoliation of PTI.

82 The charging ratio (molar [PTI framework atoms]:Na (ESI),
83 weighted M_w(PTI) = 13.14) and initial PTI loading (mg PTI/
84 mL of DMAc) are two vital factors affecting the exfoliation,
85 controlling both the yield (mass fractions of PTI) and
86 concentration of solubilised FL-PTI^{n-}. Increasing the degree
87 of charging (*i.e.* lower PTI:Na), at a static PTI loading initially
88 led to an improved yield of FL-PTI^{n-} (4.1 wt% to 34.5 wt%)
89 due to the enhanced Columbic repulsion (Fig. 2a). However,
90 further increasing charge (PTI:Na < 7) reduced the yield.
91 Similar effects have been observed in charged nanocarbon
92 solutions, attributed to Na$^+$ condensation and charge
93 screening.[11, 16] The optimum Na concentration for exfoliation
94 of PTI is 15 mM (*i.e.* 7:1 PTI:Na for 1.4 mg·mL^{-1}, Fig. 2a),
95 comparable to ~10 mM identified for the exfoliation of Na-
96 reduced graphite of similar geometry.[16] At the highest
97 charge regimes, the charge on the PTI saturates (at PTI:Na
98 ratio of ~5), as observed by the green tinge of unreacted
99 NaNp (Fig. 2a). On varying the initial PTI loading (Fig. 2b),
100 the concentration of dissolved FL-PTI^{n-} scales linearly, giving
101 a consistent yield between 31−35 wt%, indicating that there
102 may be an intrinsically soluble portion of the starting material.
103 The residue, isolated after centrifugation may contain defects
104 that bind the layers; indeed, qualitatively, the undissolved
105 residue appears disordered by SEM (Fig. S2c). The
106 maximum concentration of FL-PTI^{n-} is ~1.2 mg·mL^{-1} from a
107 PTI loading of 3.5 mg·mL^{-1}. Further increases in PTI loading
108 did not increase the concentration, indicating the solution is
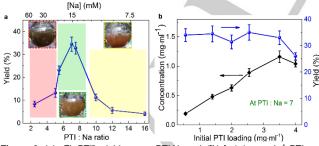109 saturated (Fig. 2b).
110

111
112 **Figure 2.** (a) FL-PTI^{n-} yield versus PTI:Na ratio/[Na], 1.4 mg·mL^{-1} PTI.
113 Yellow, green and red rectangles correspond to low, to high [Na]
114 respectively with inset photographs showing resultant FL-PTI^{n-}
115 dispersions. (b) Effect of initial PTI loading on the concentration/yield of
116 FL-PTI^{n-} dissolution (7:1 PTI:Na ratio).

117 Aqueous FL-PTI dispersions are desirable for
118 environmentally benign processing; however, pristine PTI

119 are poorly soluble in water due to their strong interlayer
120 interactions (6 h probe sonication was found to give a
121 concentration <0.2 mg mL^{-1}). The framework charging
122 process overcomes the strong interlayer interactions and
123 accelerates solubilisation in DMAc, allowing the removal of
124 the intrinsically insoluble fraction of the pristine PTI. The FL-
125 PTIs can then be recovered from the DMAc by solvent
126 exchange and the resultant FL-PTI can be transferred into
127 water by solvent exchange, reaching a saturated
128 concentration of 3.5 mg·mL^{-1}. Atomic force microscopy
129 (AFM) confirms an excellent dispersion of FL-PTI in water
130 (Fig. 3a), with corresponding heights of 0.33-3.2 nm (avg.
131 1.11 nm, Fig. 3b and S6), suggesting that the nanosheets
132 mostly comprise ~3 PTI layers, although some monolayers
133 are present. Representative energy dispersive X-ray
134 spectroscopy (EDX) maps show uniform dispersion of C and
135 N throughout the whole hexagonal area of the exfoliated FL-
136 PTI nanosheet (Fig 3c-e). High-resolution transmission
137 electron microscopy (HRTEM) micrographs show intact PTI
138 crystallites with regular hexagonal geometry and clear facets
139 (Fig. 4a). Notably, no defect holes or dislocations were
140 observed, confirming the non-destructive nature of the
141 framework charging exfoliation, as well as the high quality of
142 the starting material. The fast Fourier transform (FFT) of the
143 unfiltered HRTEM image shows a hexagonal lattice,
144 demonstrating a single crystal exfoliated FL-PTI (Fig 4a and
145 further examples in S9).[17] The minimum reciprocal lattice
146 vector, G_{min}, is 1.4 nm^{-1}, giving a lattice constant $\boldsymbol{a}$ = (2/√
147 3)G_{min} = 8.5 Å, consistent with the reported values from Br$^-$
148 intercalated PTI.[15] Two possible stacking models can be
149 considered for the FL-PTI: AB stacking with aligned voids
150 forming c-axis channels, and AC stacking without channels
151 in two adjacent layers (Fig. S10a). Comparing simulated
152 electron diffraction patterns of these two models with the
153 experimental selected area electron diffraction (SAED) data,
154 the AB stacking structure is the better fit for the FL-PTI
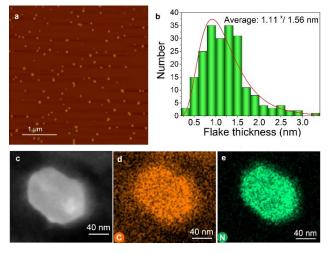155 nanosheets (Fig. 4b-d and S10b).

156

157 **Figure 3.** (a) AFM image of FL-PTI nanosheets. (b) PTI thickness
158 histogram (n>200). Mean value is derived from a lognormal distribution.
159 (c) STEM image and EDX elemental maps of C (d) and N (e) on a FL-PTI

nanosheet. The background C signal in (d) is due to the carbon TEM support.
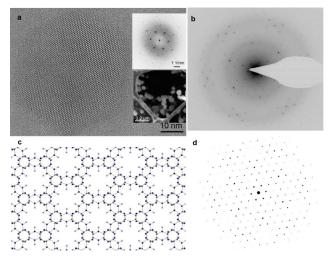

Figure 4. (a) HRTEM image of a FL-PTI nanosheet. Top inset: FFT of the HRTEM image, showing a single crystal hexagonal structure. Bottom inset: STEM image, indicating the layered structure of FL-PTI (b) SAED pattern of a FL-PTI nanosheet. (c) Schematic of the AB stacking in a bilayer. (d) Simulated electron diffraction pattern from the AB crystal structure.

The FL-PTI^{n-} synthesised in DMAc solution provides a versatile platform for covalent functionalisation of PTI, comparable to negatively charged graphene and boron nitride nanotube counterparts.[16, 18] Pristine PTI and FL-PTI nanosheets are thermally stable up to ~700 and 670˚C, respectively (Fig. 5a and Figure S12); the slightly depressed decomposition temperature for FL-PTI reflects its few-layered character. Functionalisation can be performed *via* simple addition of an alkyl halide to the reduced nanomaterial. After functionalisation by reaction with dodecyl bromide, a 10 wt% mass loss can be observed in thermogravimetric analysis/evolved-gas mass spectrometry (TGA-MS), relative to controls; the weight loss correlates with a m/z peak at 57, attributed to $C_4H_9^+$ from the grafted $C_{12}H_{25}$ alkyl chain (Fig. 5a). During the alkylation reaction, the solution changes from a clear golden, to a turbid pale yellow appearance; as the depletion of the negative charges progresses, the Coulombic stabilization is lost, leading to agglomeration and increased light scattering (Fig. 5b, S1c and S12). X-ray photoelectron spectroscopy (XPS) measurements confirmed the covalent attachment of alkyl chains to the PTI structure. Core level N 1s spectra can be divided into two components: 398.6 eV corresponding to C-N=C groups and 400.9 eV attributed to secondary and tertiary amines (NH/N-(C)$_3$) ((Figure S13 and S14).[19] An increase in the NH/N-(C)$_3$ peak was observed for the dodecyl-functionalised PTI compared to both FL-PTI and physisorption controls (Table S1). Quantitatively, the XPS data indicate 74 framework atoms per alkyl chain, comparing favourably with the TGA estimate of 101 atoms per chain. Controls of air quenched FL-PTI mixed with $C_{12}H_{25}Br$ and FL-PTI^{n-} with unreactive $C_{12}H_{26}$ showed similar TGA curves to the unfunctionalised FL-PTI, precluding a contribution from physisorption. The XPS measurements also exclude physisorption since the core level Br 3d was not observed in the grafted products, although it was visible in positive controls at relevant concentrations (Figure S15). Reaction with a shorter alkyl chain was also investigated; when charged FL-PTI reacted with octylbromide a mass loss of 12 wt% and the corresponding m/z peak at 57 were observed (Figure S16). XPS showed a similar increase in the NH/N-(C)$_3$ peak as observed for the dodecyl-functionalised PTI (Figure S17 and Table S1). In this case, XPS indicates one alkyl chain every 47 PTI atoms, closely matching the TGA estimate of one chain per 55 framework atoms. Given the uncertainties in these measurements, the agreement is excellent, and provides direct evidence of grafting to the PTI layers.
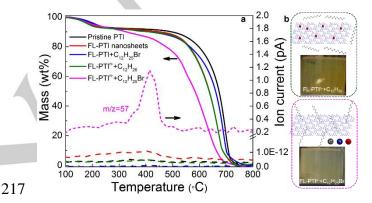

Figure 5. (a) TGA and TGA-MS (dashed) of pristine PTI and alkylated FL-PTI. Inset shows 100-400°C TGA region. (b) Photographs of control sample (top) and FL-PTI functionalised with dodecyl bromide (bottom).

The observed change in the XPS nitrogen components upon functionalization can be attributed to the attachment of alkyl chains to the nitrogen of the triazine ring. Density functional theory (DFT) calculations suggest that the sodium ion bridges two triazine rings, with the extra electron delocalized over those two rings (Figure S19). The extra electron appears to be primarily located on the nitrogen atoms of the ring, which may therefore be most susceptible to react with the alkyl bromide molecule (Scheme S2)

In summary, framework charging provides a new, simple route for exfoliation and functionalisation of PTI nanosheets, *via* NaNp/DMAc reduction. By avoiding damage, the intrinsic properties of the PTI structure can be retained and HR images indicate highly exfoliated hexagonal, crystalline FL-PTI nanosheets, averaging 1.1 nm thick (~3 layers) with AB stacking. The as-prepared FL-PTI solutions had a yield of 35 wt%, with excellent stability

y. Stabilized dispersions of FL-PTIs are useful feedstocks for a wide range of promising multifunctional applications. The small flake size is particular relevant to potential applications in (electro)catalysis and photochemistry.[20] The FL-PTI^{n-} was successfully functionalised with alkyl chains *via* the

244 framework charge, suggesting a route to a wide range of
245 functionalised species to modulate surface chemistry and
246 functional properties.

255 **Conflict of interest**

256 The authors declare no conflict of interest.

257 **References**

258

259

897; bW. R. Lee, Y. S. Jun, J. Park, G. D. Stucky, *J Mater Chem A* **2015**, *3*, 24232-24236.

[1]   J. S. Zhang, Y. Chen, X. C. Wang, *Energ Environ Sci* **2015**, *8*, 3092-3108.

[2]   M. Deifallah, P. F. McMillan, F. Cora, *J Phys Chem C* **2008**, *112*, 5447-5453.

[3]   N. Mansor, T. S. Miller, I. Dedigama, A. B. Jorge, J. J. Jia, V. Brazdova, C. Mattevi, C. Gibbs, D. Hodgson, P. R. Shearing, C. A. Howard, F. Cora, M. Shaffer, D. J. L. Brett, P. F. McMillan, *Electrochim Acta* **2016**, *222*, 44-57.

[4]   G. G. Zhang, Z. A. Lan, X. C. Wang, *Angew Chem Int Edit* **2016**, *55*, 15712-15727.

[5]   aP. Niu, L. L. Zhang, G. Liu, H. M. Cheng, *Adv Funct Mater* **2012**, *22*, 4763-4770; bS. B. Yang, Y. J. Gong, J. S. Zhang, L. Zhan, L. L. Ma, Z. Y. Fang, R. Vajtai, X. C. Wang, P. M. Ajayan, *Adv Mater* **2013**, *25*, 2452-2456; cT. Y. Ma, S. Dai, M. Jaroniec, S. Z. Qiao, *Angew Chem Int Edit* **2014**, *53*, 7281-7285; dM. J. Bojdys, N. Severin, J. P. Rabe, A. I. Cooper, A. Thomas, M. Antonietti, *Macromol Rapid Comm* **2013**, *34*, 850-854; eK. Schwinghammer, M. B. Mesch, V. Duppel, C. Ziegler, J. Senker, B. V. Lotsch, *J Am Chem Soc* **2014**, *136*, 1730-1733.

[6]   aE. Wirnhier, M. Doblinger, D. Gunzelmann, J. Senker, B. V. Lotsch, W. Schnick, *Chem-Eur J* **2011**, *17*, 3213-3221; bS. Y. Chong, J. T. A. Jones, Y. Z. Khimyak, A. I. Cooper, A. Thomas, M. Antonietti, M. J. Bojdys, *J Mater Chem A* **2013**, *1*, 1102-1107.

[7]   K. Schwinghammer, B. Tuffy, M. B. Mesch, E. Wirnhier, C. Martineau, F. Taulelle, W. Schnick, J. Senker, B. V. Lotsch, *Angew Chem Int Edit* **2013**, *52*, 2435-2439.

[8]   T. S. Miller, T. M. Suter, A. M. Telford, L. Picco, O. D. Payton, F. Russell-Pavier, P. L. Cullen, A. Sella, M. S. P. Shaffer, J. Nelson, V. Tileli, P. F. McMillan, C. A. Howard, *Nano Lett* **2017**, *17*, 5891-5896.

[9]   J. M. Englert, C. Dotzer, G. A. Yang, M. Schmid, C. Papp, J. M. Gottfried, H. P. Steinruck, E. Spiecker, F. Hauke, A. Hirsch, *Nat Chem* **2011**, *3*, 279-286.

[10]   aE. M. Milner, N. T. Skipper, C. A. Howard, M. S. P. Shaffer, D. J. Buckley, K. A. Rahnejat, P. L. Cullen, R. K. Heenan, P. Lindner, R. Schweins, *J Am Chem Soc* **2012**, *134*, 8302-8305; bP. L. Cullen, K. M. Cox, M. K. Bin Subhan, L. Picco, O. D. Payton, D. J. Buckley, T. S. Miller, S. A. Hodge, N. T. Skipper, V. Tileli, C. A. Howard, *Nat Chem* **2017**, *9*, 244-249.

[11]   A. J. Clancy, J. Melbourne, M. S. P. Shaffer, *J Mater Chem A* **2015**, *3*, 16708-16715.

[12]   N. G. Connelly, W. E. Geiger, *Chem Rev* **1996**, *96*, 877-910.

[13]   S. H. A. Axdal, D. D. L. Chung, *Carbon* **1987**, *25*, 377-389.

[14]   aS. Fogden, C. A. Howard, R. K. Heenan, N. T. Skipper, M. S. P. Shaffer, *Acs Nano* **2012**, *6*, 54-62; bA. Penicaud, C. Drummond, *Accounts Chem Res* **2013**, *46*, 129-137.

[15]   E. J. McDermott, E. Wirnhier, W. Schnick, K. S. Virdi, C. Scheu, Y. Kauffmann, W. D. Kaplan, E. Z. Kurmaev, A. Moewes, *J Phys Chem C* **2013**, *117*, 8806-8812.

[16]   T. Morishita, A. J. Clancy, M. S. P. Shaffer, *J Mater Chem A* **2014**, *2*, 15022-15028.

[17]   J. T. Yuan, J. J. Wu, W. J. Hardy, P. Loya, M. Lou, Y. C. Yang, S. Najmaei, M. L. Jiang, F. Qin, K. Keyshar, H. Ji, W. L. Gao, J. M. Bao, J. Kono, D. Natelson, P. M. Ajayan, J. Lou, *Adv Mater* **2015**, *27*, 5605-5609.

[18]   H. Shin, J. W. Guan, M. Z. Zgierski, K. S. Kim, C. T. Kingston, B. Simard, *Acs Nano* **2015**, *9*, 12573-12582.

[19]   D. Mitoraj, H. Kisch, *Angew Chem Int Edit* **2008**, *47*, 9975-9978.

[20]   aN. Mansor, J. J. Jia, T. S. Miller, T. Suter, A. B. Jorge, C. Gibbs, P. Shearing, P. F. McMillan, C. Mattevi, M. Shaffer, D. J. L. Brett, *Ecs Transactions* **2016**, *75*, 885-

WILEY-VCH

Killing two birds with one stone: Single and few-layered 2D intact crystalline carbon nitride nanosheets in an AB stacking structure were synthesized by a scalable one-pot reductive framework charging process. The novel negatively charged salt shows excellent stability under nitrogen and can be rationally functionalized by alkylation to tailor the properties of carbon nitride.

Jingjing Jia, Edward R. White, Adam J. Clancy, Noelia Rubio, Theo Suter, Thomas S. Miller, Paul F. McMillan, Veronika Brázdová, Furio Corà, Chris A. Howard, Robert V. Law, Cecilia Mattevi,* and Milo S. P. Shaffer*

Page No – Page No

Fast Exfoliation and functionalization of 2D Crystalline Carbon Nitride by Framework Charging